Earthquakes and Structures, *Vol. 8, No. 6 (2015) 1499-1528*
DOI: http://dx.doi.org/10.12989/eas.2015.8.6.1499

Effect of viscous dampers on yielding mechanisms of RC structures during earthquake

Farzad Hejazi[*1,2], Mohammad Dalili Shoaei[1,2a], Mohd Saleh Jaafar[1,2b] and Raizal Saiful Bin Muhammad Rashid[1,2c]

[1]*Department of Civil Engineering, University Putra Malaysia, 43400, Selangor, Malaysia*
[2]*Housing Research Centre, Faculty of Engineering, UPM, 43400, Selangor, Malaysia*

(Received September 14, 2014, Revised November 7, 2014, Accepted November 27, 2014)

Abstract. The yielding mechanisms of reinforced concrete (RC) structures are the main cause of the collapse of RC buildings during earthquake excitation. Nowadays, the application of earthquake energy dissipation devices, such as viscous dampers (VDs), is being widely considered to protect RC structures which are designed to withstand severe seismic loads. However, the effect of VDs on the formation of plastic hinges and the yielding criteria of RC members has not been investigated extensively, due to the lack of an analytical model and a numerical means to evaluate the seismic response of structures. Therefore, this paper offers a comprehensive investigation of how damper devices influence the yielding mechanisms of RC buildings subjected to seismic excitation. For this purpose, adapting the Newmark method, a finite element algorithm was developed for the nonlinear dynamic analysis of reinforced concrete buildings equipped with VDs that are subjected to earthquake. A special finite element computer program was codified based on the developed algorithm. Finally, a parametric study was conducted for a three-story RC building equipped with supplementary VD devices, performing a nonlinear analysis in order to evaluate its effect on seismic damage and on the response of the structure. The results of this study showed that implementing VDs substantially changes the mechanism and formation of plastic hinges in RC buildings.

Keywords: earthquake; reinforce concrete; viscous damper; seismic damage; yield surface; finite element

1. Introduction

Earthquakes, which are devastating phenomena, have always challenged, and even utterly destroyed, civil structures, while often leaving enormous casualties behind around the globe. As a direct result, structural engineers who play a primary role in designing for the safety of buildings have been proposing new techniques to tackle this crucial and unavoidable problem of human life. A thoughtful review of the methods scientists and engineers used to solve this problem from the

∗Corresponding author, Ph.D., E-mail: farzad@fhejazi.com
[a]Ph.D., E-mail: mohd.dalili@gmail.com
[b]Professor, E-mail: msj@upm.edu.my
[c]Ph.D., E-mail: raizal@upm.edu.my

 ISSN: 2092-7614 (Print), 2092-7622 (Online)

early 1970s up to the present provides us with clear insight into their basic understanding of dynamic excitation and the corresponding structural behaviour of buildings and how that improved the seismic design of structures. The initial idea for the design of buildings, either with a high level of importance or due to the existence of a dynamic load, involves taking the nonlinear behaviour of structures into account; therefore, the analysis should be sophisticated enough to show the weaknesses and deficiencies of seismically excited buildings. A large body of research, including the development of a number of analytical models, has contributed to the detection of damage and to the evaluation of the ductility of reinforced concrete (RC) structures under nonlinear cyclic or seismic loads. Meanwhile, the nonlinearity of structural members has been incorporated into the framework of finite element method which could develop its full potential for handling various aspects of two-dimensional (2D) and three-dimensional (3D) seismic structural analysis.

Schnobrich (1977) studied the nonlinear behaviour of an RC panel and slab under flexural and shear loading. Buyukozturk and Connor (1978) conducted a nonlinear analysis of RC buildings subjected to impulsive loading. Park and Ang (1985) developed a damage model of reinforced concrete members through a damage index, defined as a linear combination of large structural deformations and inelastic deformations due to cyclic loading, and evaluated the absorbed hysteretic energy. Their model has been considered and used by many researchers, including Dong, Moss, and Carr (2003), Lu and Wei (2008), Nakhaei and Ali Ghannad (2008). Dong *et al.* (2003) evaluated Park and Ang's damage model by assessing damage to an RC ductile frame and proposed a method for analytical seismic damage of RC ductile framed structures. Jiang *et al.* (2011) modified the Park-Ang model's nonconvergence deficiency at upper and lower limits. Schultz (1990) studied the nonlinear behaviour of RC frames with hinging columns, i.e., strong beam and weak column. The yielding point of the frame story was assumed when linear force-deformation relation was exceeded. Shinozuka *et al.* (1990) studied several damage control designs for RC frames such as the one based on a modified Miner's rule and a global damage model. Chandler and Mendis (2000) proposed a displacement-based approach to evaluate the ductility and displacement demands of moment-resisting (MR) frames under seismic excitation without undertaking detailed inelastic dynamic analysis. Lee and Watanabe (2003) proposed a model to predict the axial strain associated with the plastic hinge regions of RC beams under reversed cyclic loading. Krätzig and Pölling (2004) presented a 3D nonlinear stress-based elastoplastic damage model for RC members to account for plastic deformations and damage components. The plastic deformations are attributed to residual strains of the member, while the damage components originate from member stiffness degradation. Cruz and López (2004) contributed to RC frame design by proposing an approach to control the damage indices in a nominal elastic range. Légeron *et al.* (2005) developed a 2D finite-element-based, performance-based design approach which takes advantage of multilayer elements, e.g., a Bernoulli type beam, to predict seismic-origin damages of nonlinear softening RC structures. They employed damage mechanics of the RC members that took into account the cracks and confinement effect of concrete under tension and compression forces, respectively, in addition to the cyclic behaviour of the RC members.

In a nonlinear plane frame model presented by Wilkinson and Hiley (2006), the stiffness of every floor comprised the floor's assembly of beams and columns, so that displacements were defined as the sway of the floor as well as the rotation of beam-column sections. The perfectly elastic and perfectly plastic moment rotation yielding was taken into account to allow for plastic deformation and to demonstrate the collapse mechanism of plane high-rise RC frames. Inel and Ozmen (2006) evaluated the influence of plastic hinge length and the spacing of transverse

reinforcement. They showed that these properties have no effect on base shear but can change the displacement capacity of RC frames.

Erduran (2008), Athanassiadou (2008) considered the torsional effect on seismic performance of RC frames associated with eccentricity and irregularity. Mata *et al.* (2008) developed a thermodynamically consistent 3D material model for the dynamic behaviour of beam structures. Zonta *et al.* (2008) introduced a damage detection methodology based on the weak-beam/strong-column principle. The model was found capable of measuring the degradation of local stiffness at designed plastic hinges that originated from the formation of a ductile resistant mechanism. Faleiro *et al.* (2008) developed a plastic-hinge model for RC beams to localize nonlinear behaviours at both ends of the element under seismic action. Lee *et al.* (2009) proposed a model to study the effect of the axial strain of RC beams in the strength degradation of beam-column joints under seismic excitation. Grassl and Jirásek (2006), Zhang *et al.* (2010) studied 3D concrete constitutive model encompassing a combination of plasticity and damage. Triaxial damage-plastic models for the failure of concrete were presented and applied to the analysis of an RC column subjected to compressive pressure. Mohr *et al.* (2010) advanced a stress-compatible model for RC beam-column elements under shear and bending.

Several researchers, including Lee and Woo (2002), Sadjadi *et al.* (2007), Tena-Colunga *et al.* (2008), Tabatabaiefar and Massumi (2010), Mehanny and El Howary (2010), Hatzigeorgiou and Liolios (2010), have studied the seismic performance of moment-resisting RC frames buildings, accounting for the fundamental period, plastic hinge deformations, displacement ductility, interstory drift, and the damping ratio of the frames. Damage mechanisms and the structural yielding of various multistory buildings were investigated against different types of structural designs that were considered to fulfill the seismic requirements of RC structures. These studies included yield mappings of structures. Karayannis *et al.* (2011) investigated the influence of exterior beam-column joints on the global damage mechanisms of RC buildings, encompassing different aspects of structural response, like interstory drift, base shear, and the ductility requirements of beam-column joints. Xue *et al.* (2008), Habibi and Moharrami (2010), Habibi and Izadpanah (2012) came up with performance-based design guidelines for RC frame structures using a suitable design spectrum.

Akhaveissy and Desai (2012) employed a nonlinear finite element approach to modelling RC beams by integrating an eight-node isoparametric quadrilateral element and a two-node element for concrete and steel simulation, respectively, incorporating the distributed state concept and a hierarchical single yield surface to account for the fracture and failure of RC frames. Birely *et al.* (2012) developed a nonlinear RC beam model by taking advantage of two rotational springs, representing the flexural behaviour of the beam, which is governed by a moment-curvature response, and joint response, determined from the bilinear shear stress-strain relationship, namely a dual-hinge lumped-plasticity model. A similar methodology was employed by Ganjavi and Hao (2012) to study the ductility demand of structural buildings incorporating soil-structure interaction (SSI). The inclusion of SSI, as compared to fixed-base model, leads to a long fundamental period of the system, and this has been found so influential to the ductility demand distribution of the superstructure (Rajeev and Tesfamariam 2012). de Lautour and Omenzetter (2009), Lagaros and Papadrakakis (2012) used artificial neural networks to predict seismically induced damage and seismic performance (displacement) of RC frames, respectively. Artificial neural networks were also studied and used as a method to identify structural damage in RC and steel structural elements by Hakim and Razak (2013, 2014). Faisal *et al.* (2013) focused on repeated earthquakes and their corresponding effects on the story ductility demand of frame structures. Full hinge mechanism in

the structural analysis showed that the bottom stories of tall symmetric buildings are subjected to higher ductility demands than upper stories under repeated seismic disturbances.

Hueste and Bai (2007) found that a shear wall considerably enhances performance against seismic disturbance compared with other seismic retrofitting techniques. Confinement of column plastic hinges has been shown to ameliorate any strength degradation, but no considerable influence on initial stiffness has been detected. A number of researchers, including Youssef *et al.* (2007), Maheri and Ghaffarzadeh (2008), Godínez-Domínguez and Tena-Colunga (2010), have conducted experimental and numerical analyses to investigate the seismic behaviour of steel-braced RC moment frames. Investigations have shown acceptable ductility, a great capacity to dissipate energy, and less fragile steel bracing systems were provided to seismically retrofit or bolster RC frames. The collapse mechanisms of various RC frames associated with the inelastic performance of the structures were considered under seismic loading, and some guidelines for designing steel-braced RC frames were proposed. Özel and Güneyisi (2011) discussed the reductive influence of installing steel braces on the fragility index of retrofitted RC frames. V-type steel bracing reportedly leads to a better hinge pattern in the frame, with greater lateral load-carrying capacity and lower drift. Massumi and Absalan (2013) reported that not only can well-installed steel bracing provide greater stiffness, but it also increases the energy-dissipation potential of MR-RC frames. This means that the formation of plastic hinges can be significantly altered such that the collapse mechanism associated with a bare frame would not be anticipated in case of braced one.

Oviedo *et al.* (2010) presented a deformation-controlling scheme for seismic analysis of RC frame structures equipped with hysteretic dampers. They observed how drift and strength ratios assigned to hysteretic dampers influenced the performance of the considered frame structures and concluded that the reduced participation of the main frame in seismic damages and energy dissipation was achieved by selecting low values for the mentioned ratios so that the structures could sustain more inelastic cycles. Sahoo and Rai (2013) recently studied the effects of aluminium shear links, implemented as passive energy dissipation device to strengthen the seismic performance of a frame building subjected to earthquake load. Their installation prevented soft story failure by greatly improving energy dissipation, as well as by achieving the desired yield mechanism. Montuori *et al.* (2013) investigated the influence of friction dampers on the seismic behaviour of MR-RC frame structures in terms of local and global scales associated with supplementary energy dissipation and global type mechanisms, respectively. The implementation of friction dampers led to an acceptable distribution of plastic hinges and proved consistent with the global mechanism. Formulation and application of viscous damper in RC frames was presented by Hejazi *et al.* (2009), Hejazi *et al.* (2011), Hejazi *et al.* (2014) and nonlinear analysis showed improved seismic response of the considered structure.

As documented in the literature presented above, much effort has been dedicated to the investigation of seismic performance in MR-RC frame structures subjected to earthquake loading and to the capture of the structures' inelastic responses and structural failures. The research has also addressed the application of damper devices and has illustrated the consequent enhancement of the overall seismic performance of MR-RC structures. However, little research has considered how the installation of an earthquake energy dissipation system, like a damper device, would affect the occurrence of plastic damages to the structure and deformations of the structural element. Therefore, this paper presents detailed analytical procedures for analysis of an inelastic dynamic integration scheme along with computational techniques for evaluating the nonlinear responses of frame buildings. Direct step-by-step integration techniques are developed for the dynamic analysis

of RC structures equipped with earthquake energy dissipation systems, using Newmark's predictor-corrector method to solve the resulting equation of motions in the time domain. Also, the effect of damper devices on the yield surface of RC sections is considered in order to detect the damage to RC structures equipped with damper devices. Then, a computer program is codified and implemented to determine the seismic response of structures and to evaluate the effect of earthquake energy dissipation systems on the formation of plastic hinges in structural members.

2. Yielding in RC structure

Capturing the actual nonlinear behaviour of RC beams or columns subjected to external forces requires suitable modelling of the RC members. Such modelling requires developing proper criteria for plastic hinge formation under known stress states resulting from axial force and bending moment, since yielding surfaces depend on RC section properties, (Marante and Lopez 2002, Santaro and Kunnath 2013). The yield surface equation $f(p_u, m_u, p_0, m_0)$, Eq. (1), contains the ultimate axial and moment forces of the section, represented by p_u and m_u, respectively, and p_0 and m_0 stand for a sample of points with respect to the current status of axial and moment forces in the member. The equation for the interacting yield surface of an RC member, previously introduced by Thanoon *et al*. (2004) and shown in Fig. 1, was used in the current research

$$\frac{m_u}{m_0} = 1.043 + 3.842\,\frac{p_u}{p_0} - 5.731\left(\frac{p_u}{p_0}\right)^2 + 0.842\left(\frac{p_u}{p_0}\right)^3 \tag{1}$$

Therefore, during load exertion, when the induced force in an RC element falls inside the yielding surface, it means that the section remains within the elastic range; when the force of an element has reached or exceeded the yield surface, a plastic hinge has formed in the RC section.

Since the implementation of a supplemental damper device alters the RC beam or column forces during earthquake excitation, the status of a structural element with respect to yielding criteria may become altered by the force induced in the damper device, i.e., the behaviour of the

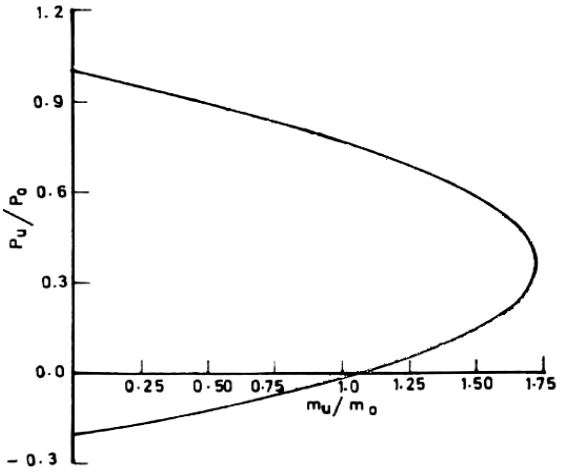

Fig. 1 RC section yield curve

RC member shifts from plastic to the elastic range. Therefore, this study has attempted to evaluate the effect of damper devices on plastic hinge formation in structural elements during dynamic excitation.

3. Modified Newmark method

This study adapted Newmark's direct step-by-step integration Newmark (1959) and the equation of motion for an elastoplastic system equipped with a viscous damper (VD). This equation is obtained through the equilibrium of forces

$$M\ddot{u}+q(u,\dot{u})=F_{VD}+F_e \tag{2}$$

where M represents the mass matrix of the system; q stands for the vector of the internal resisting forces, which depends on the displacement u and velocity $\dot{u}$; $\ddot{u}$ is the acceleration vector; Fe is the vector of the applied earthquake load; and F_{VD} is the VD force. The internal resisting forces are defined by the stiffness matrix K, the inherent damping matrix [C], and the control force originating from the VD elements. Thus, Eq. (2) can be written as

$$M\ddot{u}_{t+\Delta t}+q(u_{t+\Delta t},\dot{u}_{t+\Delta t})=F_{c_{t+\Delta t}}+F_{e_{t+\Delta t}} \tag{3}$$

where $F_{c_{t+\Delta t}}, F_{e_{t+\Delta t}}$ are the VD force and the vector of applied earthquake load, respectively, at time (t+Δt); $u_{t+\Delta t}$ and $\dot{u}_{t+\Delta t}$, the displacement and velocity of the system at time t+Δt, are defined as follows

$$u_{t+\Delta t}=\bar{u}_{t+\Delta t}+(\Delta t)^2\beta\ddot{u}_{t+\Delta t} \tag{4}$$

$$\dot{u}_{t+\Delta t}=\dot{\bar{u}}_{t+\Delta t}+\Delta t\gamma\ddot{u}_{t+\Delta t} \tag{5}$$

where $\bar{u}_{t+\Delta t}$ and $\dot{\bar{u}}_{t+\Delta t}$ are obtained from the following equations

$$\bar{u}_{t+\Delta t}=u_t+\Delta t\times\dot{u}_t+0.5(\Delta t)^2(1-2\beta)\ddot{u}_t \tag{6}$$

$$\dot{\bar{u}}_{t+\Delta t}=\dot{u}_t+\Delta t(1-\gamma)\ddot{u}_t \tag{7}$$

where β and γ are the accuracy control indices associated with the stability of the method. The quantities $\bar{u}_{t+\Delta t}$ and $\bar{\bar{u}}_{t+\Delta t}$ are the historical values, and $u_{t+\Delta t}$ and $\dot{u}_{t+\Delta t}$ are the corrector values. At the first step of the algorithm, the initial values of acceleration, $\ddot{u}_o$, must be obtained by Eq. (8) at time t=0 as

$$\ddot{u}_0=M^{-1}[(F_{VD0}+F_{e0})-q(u_0,\dot{u}_0)] \tag{8}$$

F_{VD0} and F_{e0} stand for the VD force and applied earthquake load, respectively, at time t=0. The linear analysis is done by placing Eqs. (3)-(8) into a recurrence algorithm that involves effective

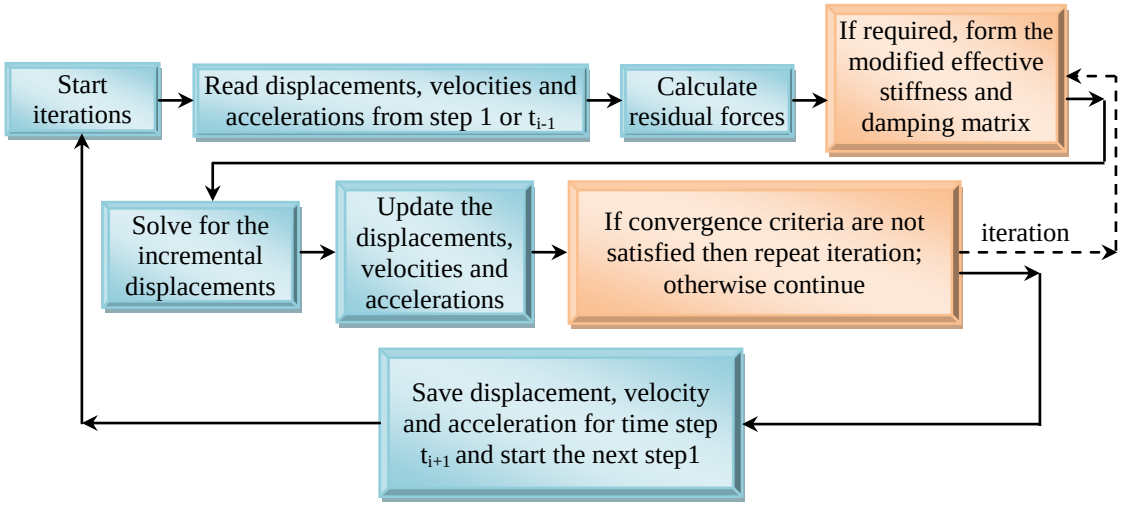

Fig. 2 The developed Newmark's algorithm for analysis of structure equipped with viscous damper

static solutions at intervals of Δt. The inelastic solution is obtained as explained above, except that the stiffness matrix is reformulated to take into account the effect of any topological change in the structure due to the formation of plastic hinges in the frame and the updating of the VD force based on velocity.

The adapted Newmark's algorithm is applied at each time step and can be summarized into the steps depicted in Fig. 2.

4. Procedure for the nonlinear analysis of frame structures equipped with VD devices

This research, in order to perform a nonlinear analysis of RC structures along with the effect of VD devices, adapted a special computational procedure to evaluate the structural member force and plastic hinge formation in the five steps described below.

Step (1): Calculation of the incremental nodal force

For any iteration, say the j^{th} iteration at time interval Δt, the incremental nodal force vector dp_j is calculated for each frame element as

$$dp_j = K_{j-1}\, du_j \tag{9}$$

where K_{j-1} is either the elastic element stiffness matrix when no plastic hinge exists at either end or the elastoplastic element stiffness matrix, provided that a plastic hinge exists at one or both element ends. The term du_j stands for incremental nodal displacement, which is obtained from dynamic analysis through modified Newmark method. The stiffness matrix may be updated, if necessary, either at each iteration or at the beginning of every earthquake loading step.

Step (2): Generation of nodal force vector

Incremental forces are added on to the converged forces of the previous step as

$$p_j = p_{j-1} + dp_j \tag{10}$$

These forces represent the nodal force vector for the element under computation. This force is due to external loads, such as imposed static and dynamic loads and damper force (if they exist). The position of each nodal force vector as a point is checked against the yield surface *f*. At this stage, the following three different conditions need to be examined:

Condition (a): Elastic stage

Satisfaction of the nodal force component, $f(p_u, m_u, p_0, m_0)<1.0$ indicates that the nodal force vector point (point O) is located inside the yield surface (*f*) and in the elastic range, as shown in Fig. 3.

Condition (b): Plastic range

If nodal force components at any node satisfy $f>1.0$, this condition is a transition from the elastic to the inelastic stage, since the nodal force point has jumped outside the yield surface (from point O to point B in Fig. 3). The condition, $f>1.0$, represents an inadmissible state, since an RC section cannot resist the computed forces, which are now more than the ultimate strength state. These nodal forces need to be brought on to the yield surface to satisfy $f=1.0\pm\varepsilon_r$, where ε_r is an error limit taken as being equal to 0.1 percent in this study. This was done to dissipate some of the earthquake energy by the VD device. In this case, three different conditions may occur, as follows:

i. Adding a VD device to the considered point. By implementing the VD force (dF_j), the supplemental damper dissipates the forces in the structural members due to earthquake, and the force location is returned from outside (point B) to the inner side of the yield surface as shown by point C in Fig. 3, which means that the nodal loads are decreased and the nodal force components is satisfied ($f<1.0$) for all elements. The structure is again in the elastic range, and the analysis continues.

ii. If a VD device exists at the considered location already, VD damping properties are changed in order to dissipate the seismic load and return the point (B) to the inside of the yield curve.

iii. After implementing the VD system or changing the existing damper properties, the point may still be outside of the yielding surface ($f>1.0$). This indicates that the RC frame cannot resist the computed forces even by utilizing the earthquake energy dissipation system. Again, these nodal forces need to be brought on to the yield surface to satisfy $f=1.0$, and it is possible by allowing an inelastic deformation to proceed normal to the yield surface, which will result in unbalanced forces that will be redistributed in the next iteration.

The procedure used to bring a point located outside the yield surface back on to the yield surface (from point B to point C in Fig. 3) is explained in what follows.

(a) Find the location of point A on the yield surface by calculating a scalar factor *R* such that

$$f(p_{j-1} + (1-R)dp_j) = 1.0 \pm \varepsilon_r \tag{11}$$

Having determined the value of *R*, calculate the total element nodal forces which satisfy the yield criterion (at point A) as

$$(p_j)_A = p_{j-1} + (1-R)dp_j \tag{12}$$

(b) Using the nodal force vector at point A, calculate the *G* matrix. Next, find the flow constant

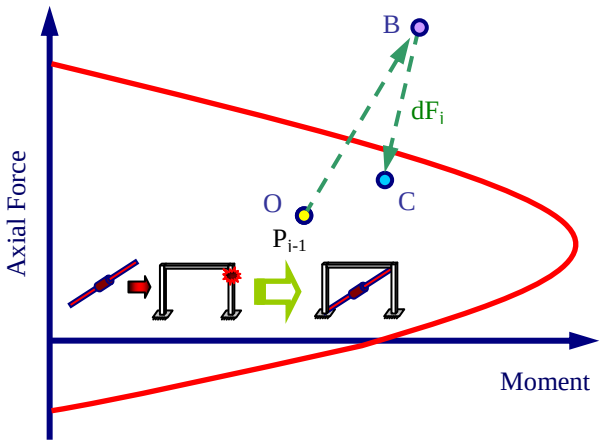

Fig. 3 Shift the point from outside to inside of yield surface by implementation viscous damper

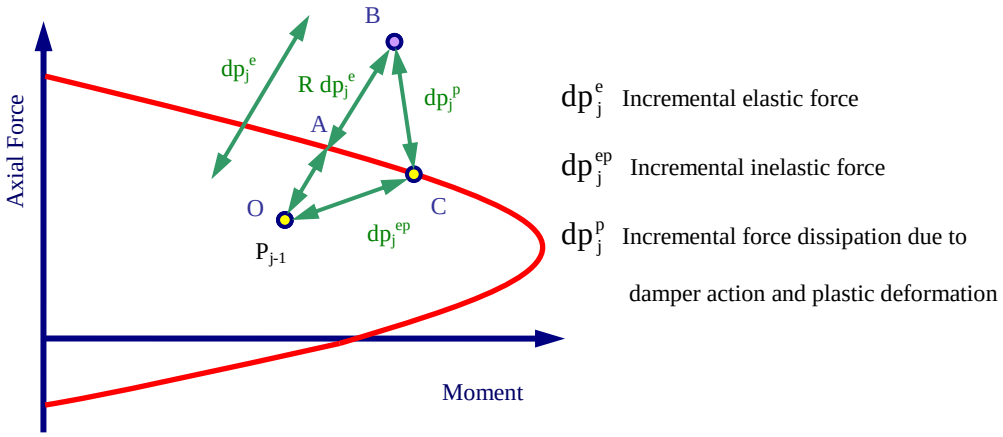

Fig. 4 Inelastic redistribution of force

λ for the inelastic deformation part ($R\ du_j$). These two parameters (G, λ) are used to find plastic deformation vector as

$$du_j^p = \lambda_k G_k \tag{13}$$

(c) Find the incremental force dissipation vector dp_j^p due to the plastic deformations as

$$dp_j^p = K_e\, du_j^p + dF_j \tag{14}$$

(d) Calculate the final force state at the element ends as now lying at point C, shown in Fig. 3, by using the following relation

$$p_j^{ep} = P_{j\text{-}1} + dp_j - dp_j^p \tag{15}$$

This expression is illustrated vectorially in Fig. 4. These forces may depart somewhat from the yield surface, as the figure shows. This discrepancy can be minimized by ensuring that the load increments (or time step) adopted in the analysis are sufficiently small.

Condition (c): A plastic hinge exists at the end

If there is a plastic hinge at one or both ends of the element prior to the current iteration, any one of the following conditions may occur:

I. The nodal forces at the plastic hinge end satisfy f=1.0,

II. The nodal forces at the plastic hinge end satisfy f>1.0,

III. The nodal forces at the plastic hinge end satisfy f<1.0.

So, a plastic hinge in the previous step (or iteration) exists at either end of the element; the position of the force state with respect to the yield surface needs to be examined:

i. If the force state satisfies the condition, f=1.0 (the point moves on the yield surface), the solution proceeds as in the elastic case, except for using the elastoplastic stiffness matrix instead of the elastic stiffness matrix, thereby taking into consideration the presence of a plastic hinge. This situation ensures that no further forces are to be distributed at the plastic hinge end. Due to the rotation of the plastic hinge, the position of the neutral axis (or curvature) of the concrete cross-section gets altered, while the top fiber strain is assumed to remain equal to the ultimate concrete strain.

ii. In case f>1.0 at a plastic hinge zone, the point again jumps outside the yield surface. A procedure similar to that given for the condition (b) is followed to bring the point back on the yield surface by adding or changing the VD or considering plastic hinge occurrence. The only difference being that the scalar constant R is taken as equaling 1.0. This condition usually occurs in a dynamic analysis, such as an earthquake time history analysis, since inertia forces, seismic load, and damper power come into the computational process and affect the forces in the plastic hinge zone.

iii. When f<1.0 at a plastic hinge end, an unloading condition is indicated, due to reducing the earthquake load or VD operation; again, an elastic analysis is carried out. Determining the value of the flow constant λ, since it changes sign from positive to negative in case of unloading, can be used to cross-check for the unloading situation.

Step (3): Compute the structure's resisting forces

The final nodal force vector obtained in step (2) is converted to the global coordinate axes by a proper transformation, as follow

$$\overline{P}_j = T^T \times P_j \times T \tag{16}$$

where P_j is the final local nodal force vector, $\overline{P}_j$ is the final global nodal force vector, and T is the diagonal transformation matrix. Therefore, by adding the similarly obtained forces from the elements to the final global nodal force vector, the total neighbouring resisting forces developed in the structure are computed

$$\Psi_j = \sum_{e=1}^{Element\,Number} \overline{P}_{ej} \tag{17}$$

where Ψ_j is total resisting force.

Step (4): Calculate residual forces

The residual forces caused by the formation of a plastic hinge in any iteration are calculated as the difference between the applied load vector and the resisting force vector

$$R_j = Fe_j - \Psi_j \tag{18}$$

where R_j is the residual force and Fe_j represents the applied force vector in the j^{th} iteration.

Step (5): Analysis of structures

The residual force vector is then applied to the structure, and the structure is reanalyzed after modifying the stiffness matrix (if required) to take into account the formation of any new plastic hinges during the previous iteration. The procedure is repeated over a number of iterations, until a specified convergence condition is satisfied. The flowchart of the overall elastic and inelastic dynamic analysis of a structure with a supplemental earthquake energy dissipation system is shown in Fig. 5.

5. Plastic deformation

In classical theory of plasticity, the flow rules state that the plastic deformation rates are linearly related to their corresponding force (or stress) rates. Therefore, the associated flow rule presented in Eq. (13) relates the plastic component of the incremental nodal displacement at node k (k=i, j) of the beam element with λ_k and G_k which are the flow constants and the gradient vector of the yield surface at beam end k (k=i, j), respectively. The vector of G_k can be expressed as the following

$$G_i = \{G_i\} = \left\{ \frac{\partial f}{\partial p_1} \;,\; \frac{\partial f}{\partial p_2} \;,\; \frac{\partial f}{\partial p_3} \;,\; \frac{\partial f}{\partial p_4} \;,\; \frac{\partial f}{\partial p_5} \;,\; \frac{\partial f}{\partial p_6} \right\}^T \tag{19.1}$$

$$G_j = \{G_j\} = \left\{ \frac{\partial f}{\partial p_7} \;,\; \frac{\partial f}{\partial p_8} \;,\; \frac{\partial f}{\partial p_9} \;,\; \frac{\partial f}{\partial p_{10}} \;,\; \frac{\partial f}{\partial p_{11}} \;,\; \frac{\partial f}{\partial p_{12}} \right\}^T \tag{19.2}$$

For an element, to have plastic hinges at its both ends, the flow rule may be expressed as

$$du^p = \begin{Bmatrix} du_i^p \\ du_j^p \end{Bmatrix} = \begin{bmatrix} g_i & 0 \\ 0 & g_j \end{bmatrix} \begin{Bmatrix} \lambda_i \\ \lambda_j \end{Bmatrix} = G\{\lambda\} \tag{20}$$

Assuming that the element deformation increments can be decomposed into an elastic component and a plastic component

$$du = du^e + du^p \tag{21}$$

The element resists the elastic component of the displacement, creating incremental nodal forces dp as presented by Eq. (9). The element forces are uniquely determined by the element elastic nodal displacement. Therefore, this equation can be written as

$$dp = K_e\left(du - du^p\right) \tag{22}$$

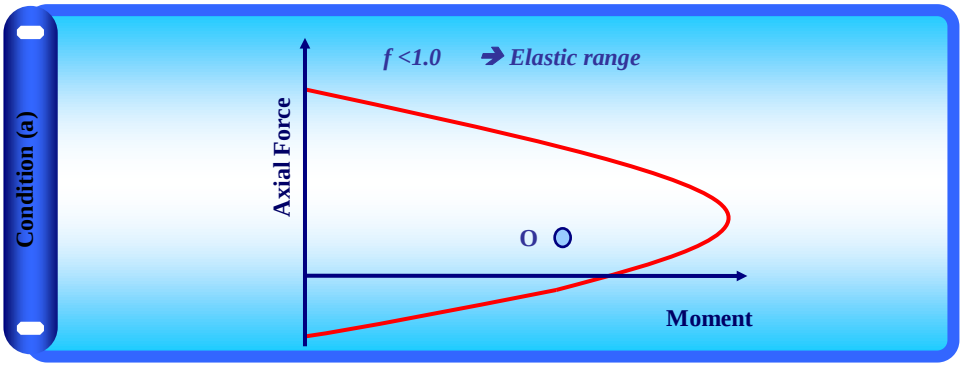

(a) Condition a

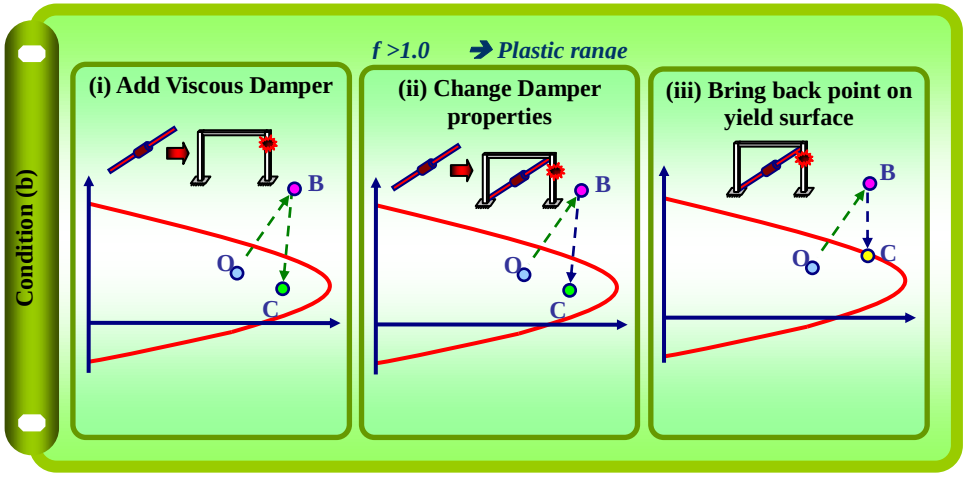

(b) Condition b

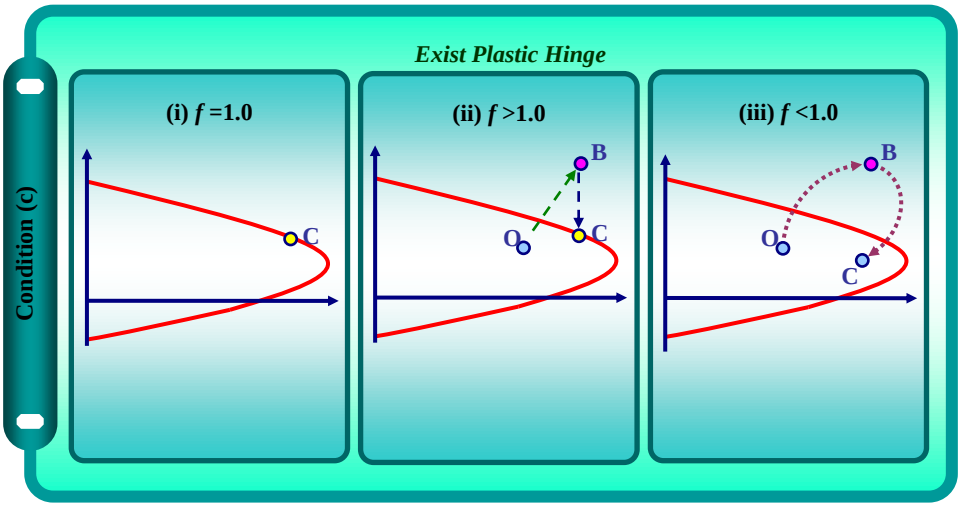

(c) Condition C

Fig. 5 Various conditions of force stating with yield surface

K_e is elastic stiffness matrix. So by substituting the value of du^p from Eq. (20) in Eq. (22), d_p is equal to

$$dp = K_e du - K_e G\{\lambda\} \tag{23}$$

Premultiplying both sides of the above equation by G^T could reach to

$$G^T dp = G^T K_e du - G^T K_e G\{\lambda\} = \{0\} \tag{24}$$

Solving this equation for $\{\lambda\}$, the flow constants get expressed as

$$\{\lambda\} = \left[G^T K_e G\right]^{-1} G^T K_e du \tag{25}$$

Since the plastic work is positive, the flow constant $\{\lambda\}$ must be positive if the element is to keep on loading. A negative term in $\{\lambda\}$ indicates an attempted elastic unloading. Putting the value of λ in Eq. (23) will get

$$dp = K_e du - K_e G\left[G^T K_e G\right]^{-1} G^T K_e du \tag{26}$$

or,

$$dp = K_e du + K_p du = K_{ep} du \tag{27}$$

Where K_p is the plastic reduction matrix

$$K_p = -K_e G\left[G^T K_e G\right]^{-1} G^T K_e \tag{28}$$

K_p represents the loss of the elastic stiffness K_e due to the development of plastic hinges at one or both ends of the beam-column element. For fully elastic element, K_p is a null matrix. The K_{ep} matrix may be expressed as

$$K_{ep} = K_e + K_p \tag{29}$$

K_{ep} the elasto-plastic element stiffness, represents the reduced, elastic stiffness of the element resulting from the constraint that yield must follow the yield surface, considering the current condition of stress resultants.

6. Development of the computer program

The algorithms described in the previous sections have been codified with FORTRAN into a computer program and a special finite element program has been developed for the Nonlinear Analysis of Reinforced Concrete Buildings Equipped with Earthquake Energy Dissipation System NARCBEEEDS (2012). There are several types of dampers that may work pretty much well in reduction of seismic forces induced in the structural elements. Each may have better functionality over another one, depending on the situation. In practice, even the nonlinear dampers can be more useful and more efficient. It is needed to highlight that the developed finite element algorithm and program code are applicable to nonlinear damper too. The developed program can perform the analyses described below.

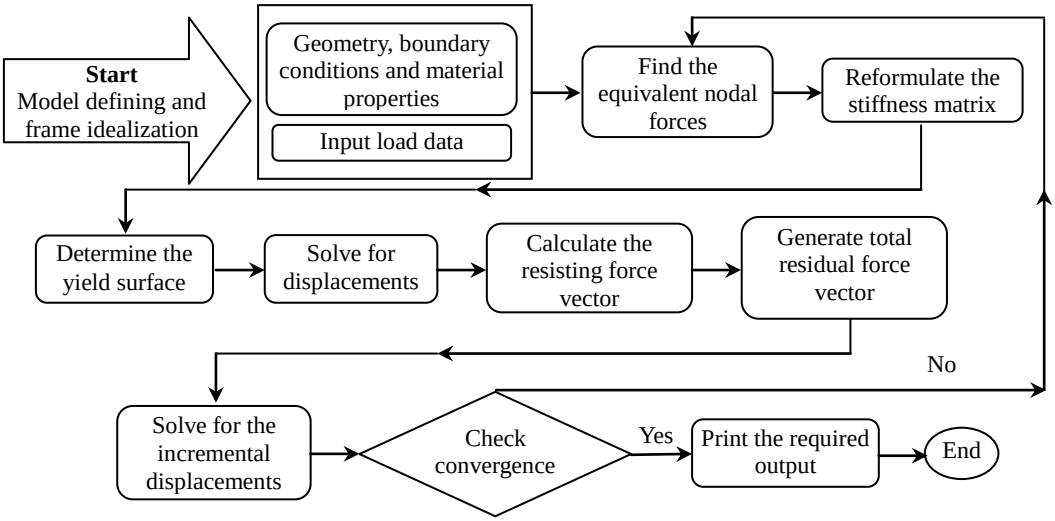

Fig. 6 Flowchart of analysis of RC building using NARCBEEEDS finite element program

I. Nonlinear dynamic analysis;

II. Modelling of 3D structures;

III. Using a two-node nonlinear frame element with two plastic hinges at its ends to model beams and columns;

IV. Modelling an inelastic VD element with nonlinear function; and

V. 3D dynamic excitation, such as earthquake (two independent horizontal and a vertical ground motion)

The developed program can be executed in Fortran Power Station 4.0 compiler using Microsoft's Developer Studio.

The procedure for analyzing an RC frame building with a supplemental energy dissipation system using the developed program code is shown in the Fig. 6 flowchart. The data input to the program comprises section geometry, number of segments, material properties, nonlinear constants, damper properties, and applied static and dynamic (earthquake) loads. This program deals with forces and moments rather than stresses. Some further details follow.

i. The program checks yielding that may occur at the ends of any element.

ii. It calculates the inelastic forces to be redistributed in the next iteration.

iii. It calculates the plastic deformations.

iv. It calculates the stiffness matrix, considering the current state of stress resultants.

v. It calculates the VD damping force and modifies it in each iteration, based on the optimum control system.

7. Verification of nonlinear analysis

To test the performance of the developed program in predicting the inelastic behaviour of the frame, a simple portal RC frame analyzed by Thanoon (1993), shown in Fig. 7 is selected. The same figure also shows the dimensions of the frame together with the cross section and the reinforcement details. The frame was first statically analyzed for dead load and live load, which

are assumed to be uniformly distributed (30 kN/m) on the beam (Fig. 8(a)). The resulting internal forces and moments were considered as the initial forces for the next nonlinear analysis.

The frame was analyzed for a horizontal load of 200 kN applied at joint (2), as shown in Fig. 8(b). The load was applied in small steps, and a nonlinear static analysis was carried out. Fig. 9 shows the sequence and location of plastic hinges occurring in the frame during application of the horizontal load. Fig. 10 shows the load-deflection curve for the joint (2), along with the curve obtained from Thanoon (1993); very close agreement was observed. The corresponding deflection

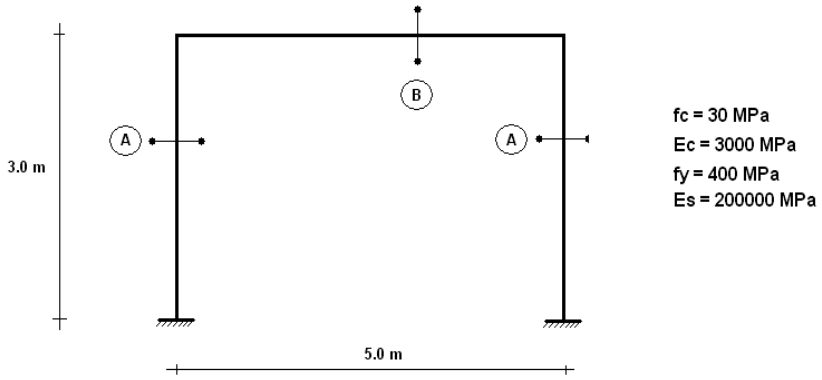

(a). RC frame

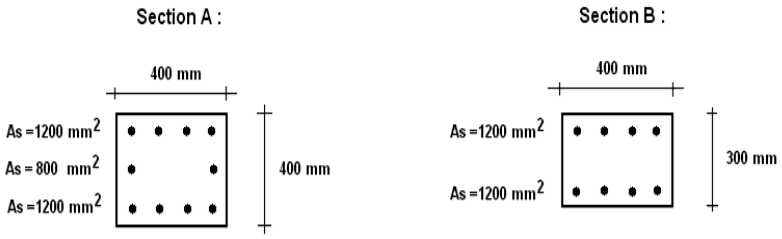

(b). beam and column section

Fig. 7 Portal RC frame (Thanoon 1993)

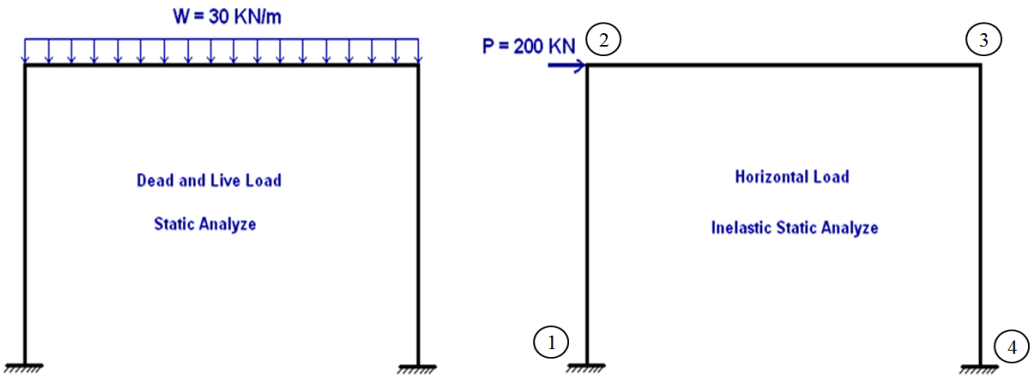

(a)-Dead load (b)-Horizontal load

Fig. 8 Loading on frame

and load factor for plastic hinges are shown in Table 1, as computed by the developed program. Comparison shows for plastic hinges formed at the loading steps with load factors of 0.85, 1.0 and 1.176, the displacement of joint (2) has the percentage error of 8.2 percent, -1.8 percent and -0.98 percent respectively. The results are almost identical, with marginal differences due to the computer's computation error. Similar trend for inelastic response of a 3D RC frame has been reported by Thanoon *et al.* (2004).

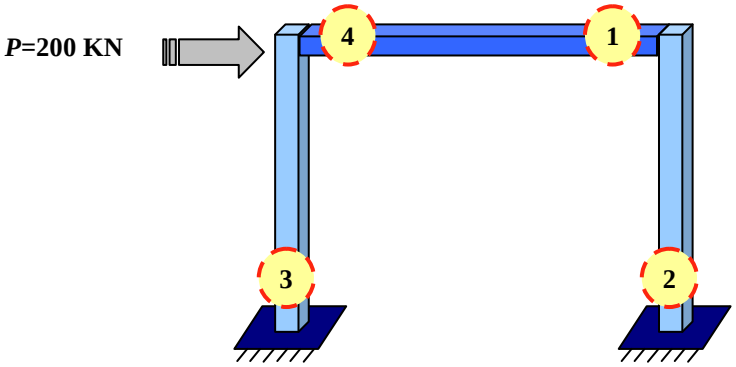

Fig. 9 Sequential formation and location of plastic hinges

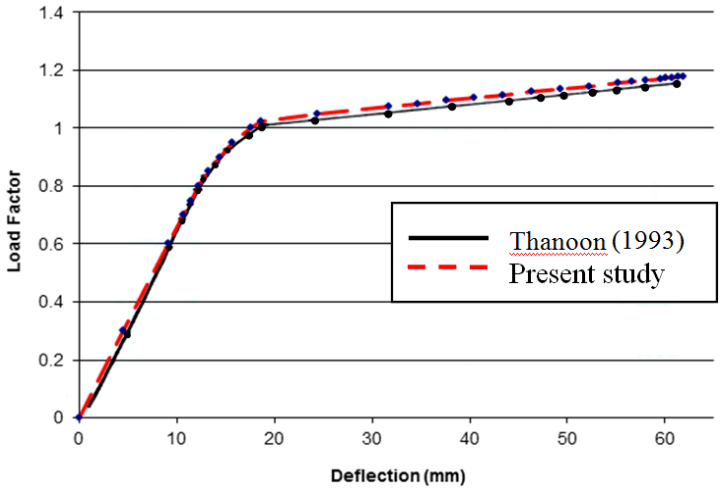

Fig. 10 Inelastic response of deflection in different load increments

Table 1 Sequence of plastic hinge formation and corresponding deflection and load factor

Thanoon (1993)			Present study		
Plastic Hinge	Deflection (mm)	Load Factor	Plastic Hinge	Deflection (mm)	Load Factor
1	13.27	0.85	1	12.22	0.75
2	15.64	0.95	2	14.41	0.85
3	18.95	1.025	3	18.61	1.00
4	62.5	1.18	4	61.89	1.176

8. Computational procedure

Conducting the nonlinear dynamic analysis required initially performing a linear static analysis to apply static loads (live and dead loads) to the structure. In the first analytic phase, the concrete and steel material properties, beam/column section geometries, and damper parameters were defined; then, structural geometry and damper configurations were modelled by defining the nodes and element connectivity. The stiffness matrix of the structure was obtained by assembling beam and column stiffness matrices.

Eventually, static loads, including gravity, and dead and live loads were applied to the structure; element forces, due to static loads, were determined and used in the second phase (dynamic analysis) as initial member forces. In the second phase, the structure was subjected to seismic load. Therefore, the structure was excited using a time-history acceleration of earthquake, and a nonlinear dynamic analysis was carried out. Each time step of the dynamic load excitation was subdivided into sub time steps, in which stiffness, the damping matrix, and the damper force vector got updated.

The following summarizes and explains the design process for an RC frame structure equipped with the developed VD system:

I. The building was modeled using the finite element program, and the beams and columns were designed.

II. Static loading, including dead and live loads, was imposed to structure model; a static analysis was undertaken to compute the internal force of the beams and columns as the initial force for dynamic analysis.

III. Nonlinear dynamic analysis of the model was performed by subjecting the structure to 3D earthquake excitations.

IV. The response of the building was checked for the occurrence of plastic hinges, and structural displacement was checked for design criteria. If the structure's seismic response was accepted, the design was considered complete. Otherwise, the process continued to the next step.

V. VDs were added, or existing VD properties were changed, and the design process resumed at step (II). This procedure was repeated until the structure's seismic response satisfied the design criteria in step (IV). If adding a VD or changing the existing VD parameters couldn't satisfy the design criteria, the beam or column section was changed.

Fig. 11 shows the overall computation procedure. This procedure facilitated the design of the RC structure; the developed system made it possible to estimate and prevent structural damage and to redesign until the model could satisfy the desired design criteria.

9. Parametric study of three-story RC building

In order to evaluate the effect of a VD device on seismic damage to buildings, the three-story RC structure shown in Fig. 12 was considered and modelled using the developed finite element program. The considered RC frame was first designed according to Eurocode.

The sections and material properties are depicted in Fig. 13. The distributed load on beams was considered to be 25 kN/m, and the concentrated load on columns was 40 kN. The structure was subjected to the El Centro earthquake record (1940, USA) in three dimensions, namely, North-South, East-West, and up-down (Fig. 14).

After performing a dynamic plasticity analysis of the structure, seismic damage to the structural

elements was evaluated. The result indicated that 86 plastic hinges were formed in structural elements during both earthquake excitation and unloading. Some of the plastic hinges were removed from members, which shows that the state of the force in the RC section shifted from the yield surface to the inside of the curve and led to the removal of the plastic hinges.
In addition, under the considered seismic load, the state of the force moved to the outside of the yield surface, and plastic hinges formed again. In total, 384 plastic hinges appeared in structural elements due to loading and unloading. The locations and sequence of occurrence for the first 50 plastic hinges in the structure modeled without a VD device are shown in Fig. 15. After that, VDs

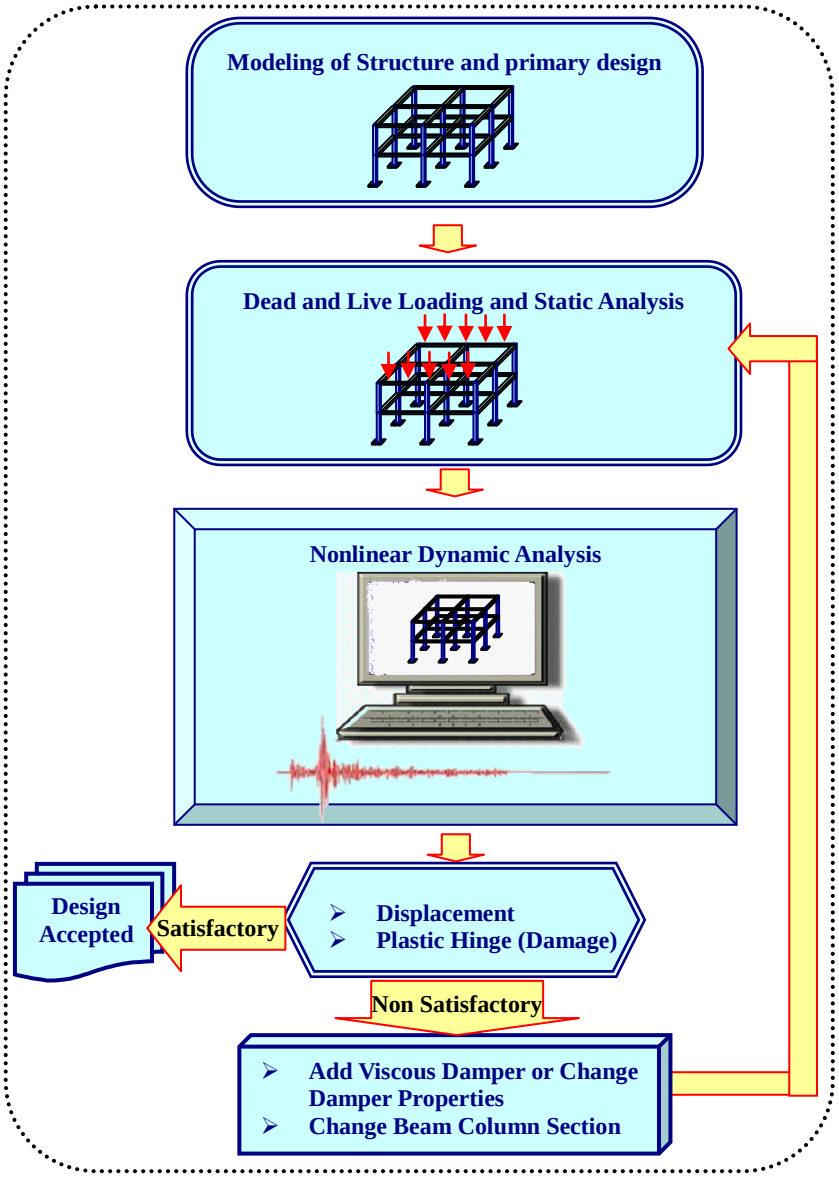

Fig. 11 The computational procedure for analysis and design of reinforced concrete frame structure with earthquake energy dissipation system

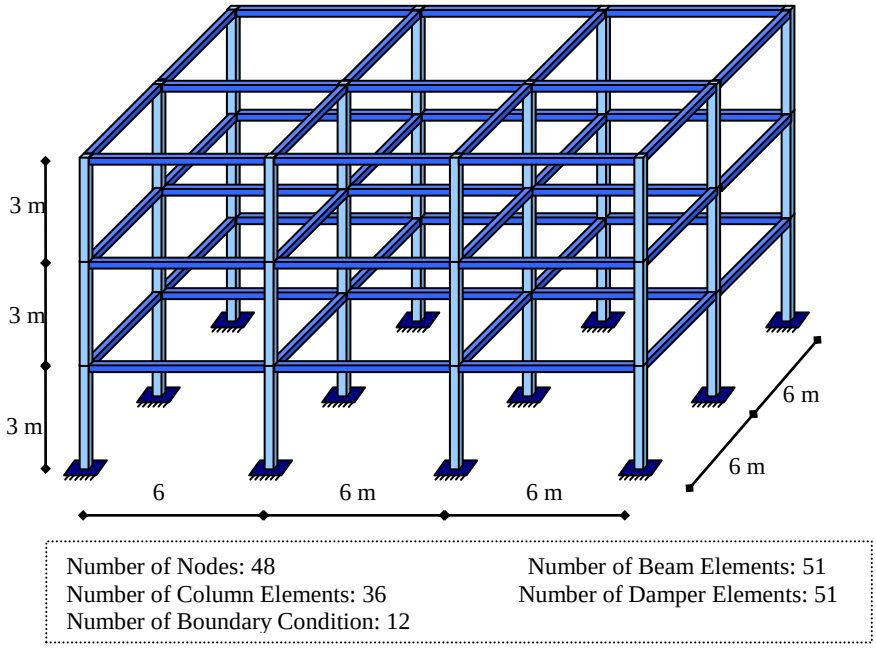

Fig. 12 Geometry of the 3D three-story reinforced concrete frame structure

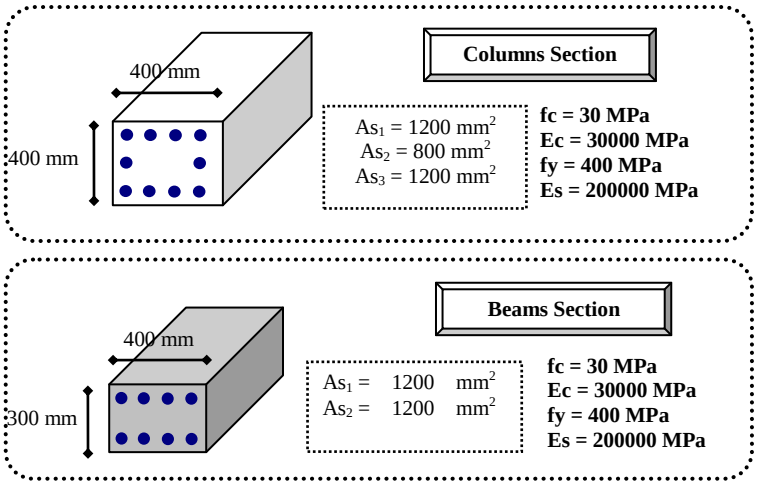

Fig. 13 Beam, column cross sections and material properties

were added to all surrounding bays in all stories of the frame, as shown in Fig. 16. Practically, arrangement and location of dampers should be consistent with architectural aspect of construction. The selected dampers location in the frame allows for openings like door and windows as shown in Fig. 16(b). It should be highlighted that location of damper can change inelastic structural performance of the frame. In case the effect of arrangement of damper device in plastic response of structure during earthquake excitation is concern, it is possible to implement

the present finite element algorithm for such purpose.

The performance of damper and damping of the damper depends on mechanical properties of damper such as size of damper cylinder and piston and viscous fluid material properties. Therefore, in order to obtain the desired damping, viscous damper has to be designed. Several researchers such as Constantinou and Symans (1993), Makris *et al*. (1993), Soong and Constantinou (1994), Hwang (2000) have addressed the mechanical properties of viscous dampers. In order to evaluate the effect of damper properties on seismic damage to the building, a parametric study was done of the VDs' performance with various damping coefficients and 5% of damping ratio, and a nonlinear dynamic analysis of the RC frame was carried out for the range of 50 to 900 kN.sec/m damping coefficients.

The numbers of sections which experienced plastic hinge formation and total plastic hinge occurrence in the structural element during loading and unloading of the earthquake load for various VD damping coefficients are plotted in Fig. 17. As can be seen in this figure, the use of a VD with C=900 kN.sec/m was able to reduce the number of sections which yielded due to plastic hinges formation to 14 from 86, when no VD device was installed.

Therefore, the use of a damper device prevented 72 section plastic hinges (83 percent reduction). Repetitions of plastic hinge occurrence in beam and column sections during earthquake (total plastic hinges) decreased from 384 times to 21 when C=900 kN.sec/m, which amounts to a 94 percent reduction in plastic hinge formation. Increasing the damping coefficient increases damper power; therefore, more of earthquake's energy gets dissipated by VD. As seen in Fig. 17, increasing the damping coefficient reduces the number of section plastic hinges and total plastic hinges.

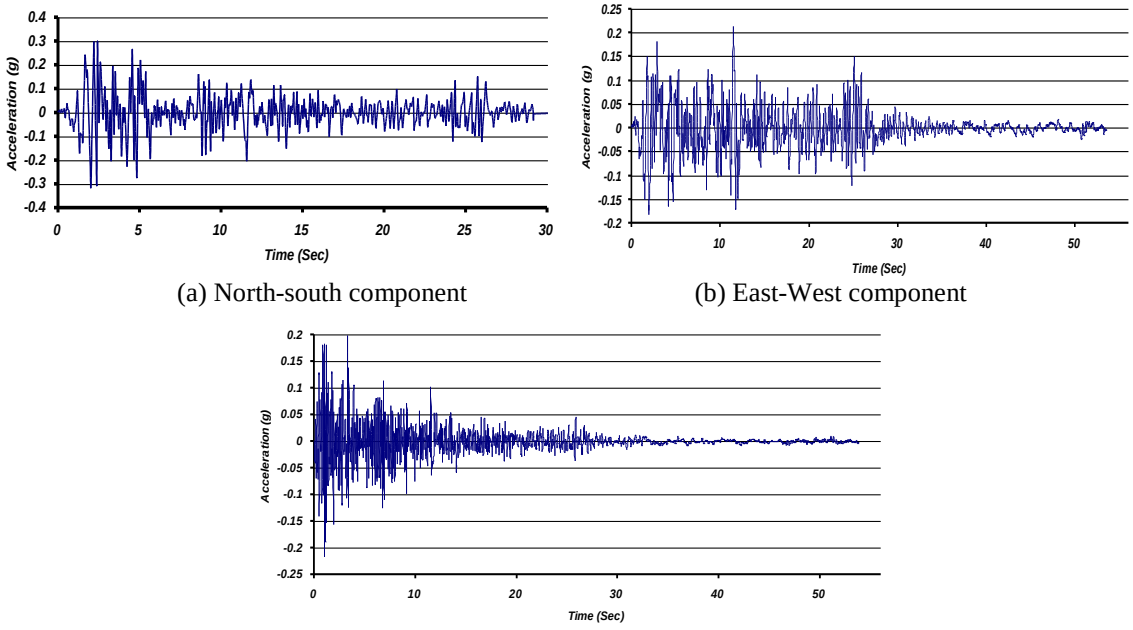

(a) North-south component (b) East-West component

(c) Up-down component

Fig. 14 Earthquake acceleration record components of El Centro (Imperial Valley Irrigation District, USA-1940)

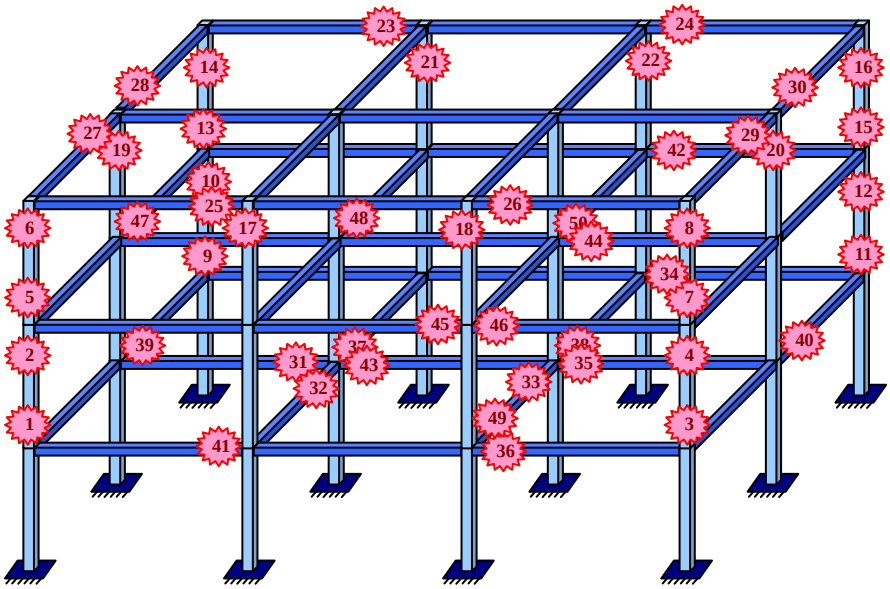

Fig. 15 Location and sequence of plastic hinge occurrence during earthquake excitation

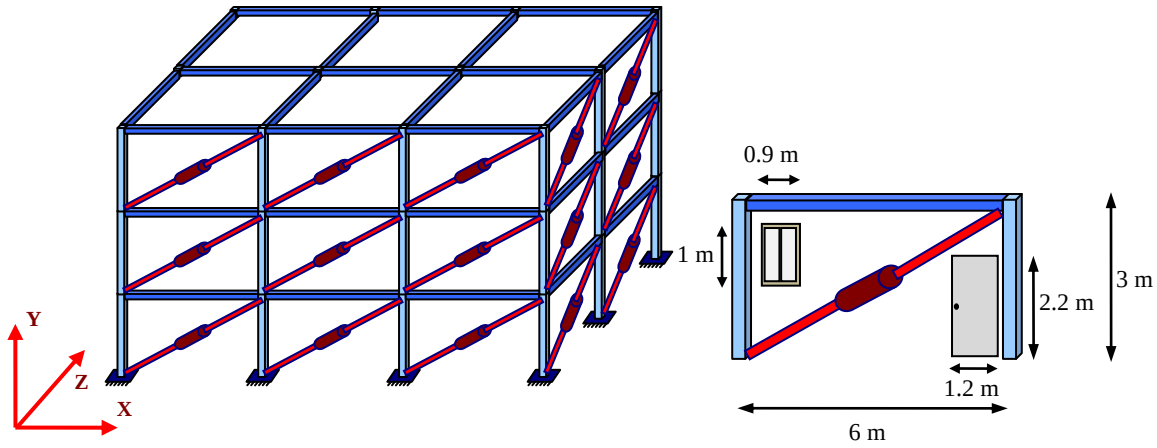

(a) arrangement of dampers (b) schematic architectural view

Fig. 16 The considered frame and position of viscous damper device

Fig. 18 depicts the results of an inelastic analysis in terms of peak displacements of structural nodes in three dimensions - two horizontal (*X* and *Z*) and one vertical (*Y*). It is obvious from Fig. 18(a) and 18(b) that the peak horizontal displacements of the structure are reduced by increasing the damper damping coefficient. A VD with *C*=900 kN.sec/m reduced the peak horizontal amplitude of the structure in direction *X* from 32.2 mm to 2.6 mm; the damper device diminished the *X* direction movement by 92 percent. This type of damper decreased the peak horizontal amplitude in direction *Z* from 34 mm to 2.7 mm, which equals a 92 percent reduction.

Also, as seen in Fig. 18(c), raising the damper damping coefficient leads to the degradation of vertical displacement magnitudes in cases where *C*=50 to 400 kN.sec/m. This highlights the fact

that analysis of a structure should consider various damping coefficients and that the 3D seismic response has to be evaluated to find the optimum VD parameters in order to minimize a structure's response during earthquake excitation. The maximum vertical reduction found was 50 percent when *C*=900 kN.sec/m; the peak vertical movement was reduced from 2 mm to 1 mm. Peak rotations of structural nodes are plotted in Fig. 19. The graphs show that, similar to the displacements, the amplitudes of rotations were reduced by increasing the damping coefficient. However, for some damping coefficients, the trend of reduction in rotation amplitude did not occur as predicted, since enhancing the damping coefficient increased the rotation amplitude.

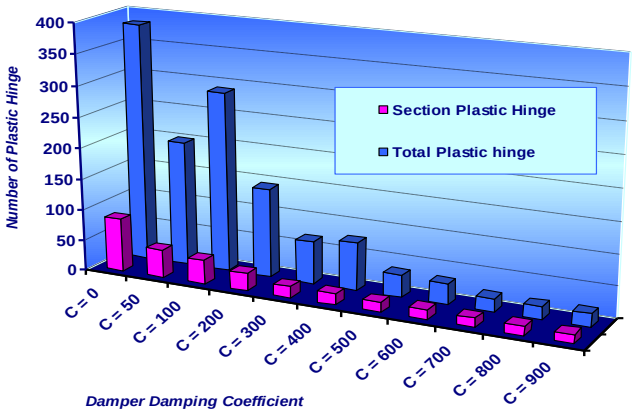

Fig. 17 Number of plastic hinge against different damper damping coefficient

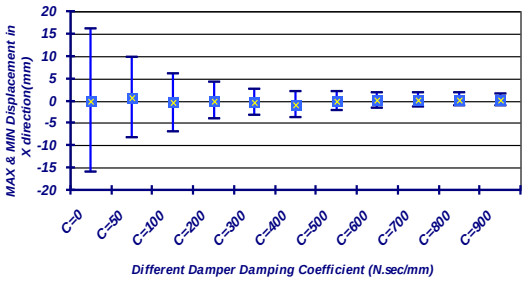

(a) *X* direction

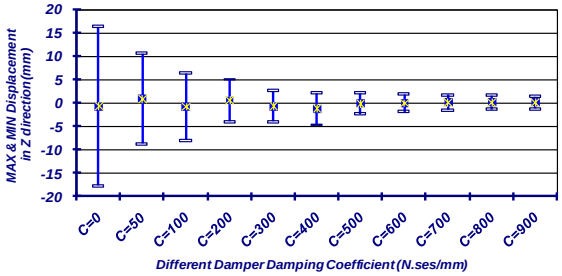

(b) *Z* direction

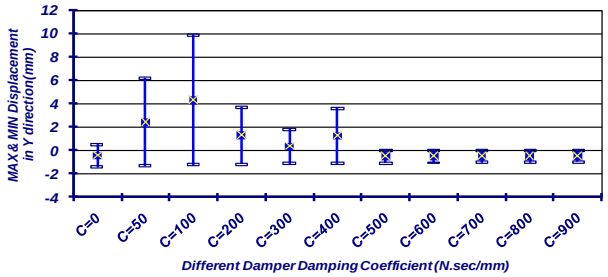

(c) *Y* direction

Fig. 18 Peak maximum & minimum displacement of structure nodes for different damping coefficient

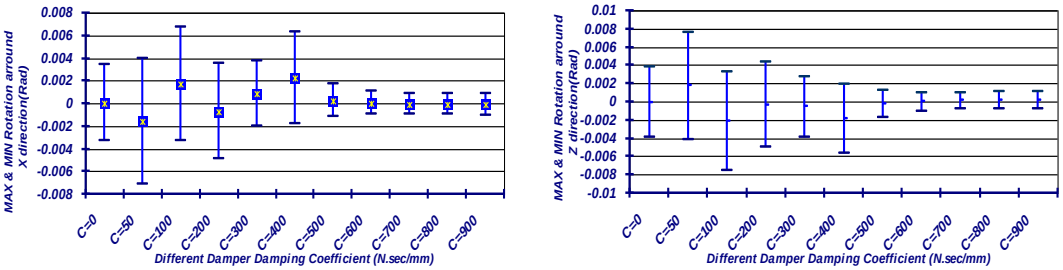

(a) *X* direction (b) *Z* direction

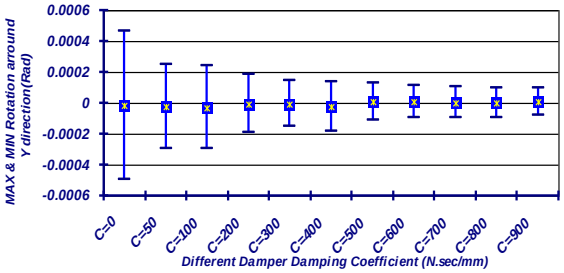

(c) *Y* direction

Fig. 19 Peak maximum and minimum rotation of structure nodes in different damping coefficient

Fig. 20 shows the peak axial and shear forces in all beams and columns for different damping coefficients. As shown in Fig. 20(a), the range for peak compression and tension, the negative and positive axial force, respectively, in structural members (beams and columns) degrades as the damping coefficient increases. The peak compression and tension forces in structural members with no VD (C=0) are 16.13 kN and 16.14 kN, respectively. The forces decrease to 1.4 kN and 1.25 kN when a supplemental VD with a damping coefficient equal to 900 N.sec/mm is used. The VD (C=900 N.sec/mm) reduced the peak compression and tension forces in structures by 91.31 percent and 92.2 percent, respectively.

Fig. 20(b) shows the peak shear forces in direction Z in beams and columns for different damping coefficients. As seen in this figure, the peak shear force in direction Z decreased from 34.09 kN to 2.7 kN (a 92 percent reduction). Fig. 20(c) depicts shear force variations around direction Y using different damping coefficients. The range of peak shear force in direction Y increased from 2 kN for the structure without a VD to 11.18 kN for the structure equipped with a VD C=100 kN.sec/m and again reduced to 1.01 kN in case of a damping coefficient equal to 900 N.sec/mm, which equals a reduction of about 50 percent. Clearly using a VD sometimes increases a structural member's force, and through structural analysis of various damping coefficients, the most effective damper can be selected.

The peak amplitudes of the torsion forces at various damper damping coefficients are shown in Fig. 21. As seen in the plot, torsion peak amplitude increases from 6.7 kN.mm in structure without damper C=0 kN.sec/m to 11 kN.mm through the use of damper with damping coefficient of C=50 kN.sec/m. This amount decreases to 9.9 and 8.4 kN.mm with 100 and 200 kN.sec/m damping coefficients, respectively. The greatest reduction, observed when C=900 kN.sec/m, is 1.9 kN.mm and it reflects a 71 percent improvement.

Fig. 21(b) shows the peak moment variation around direction Z for the considered damping coefficients. The peak amplitude of moment around direction Z in structure without the

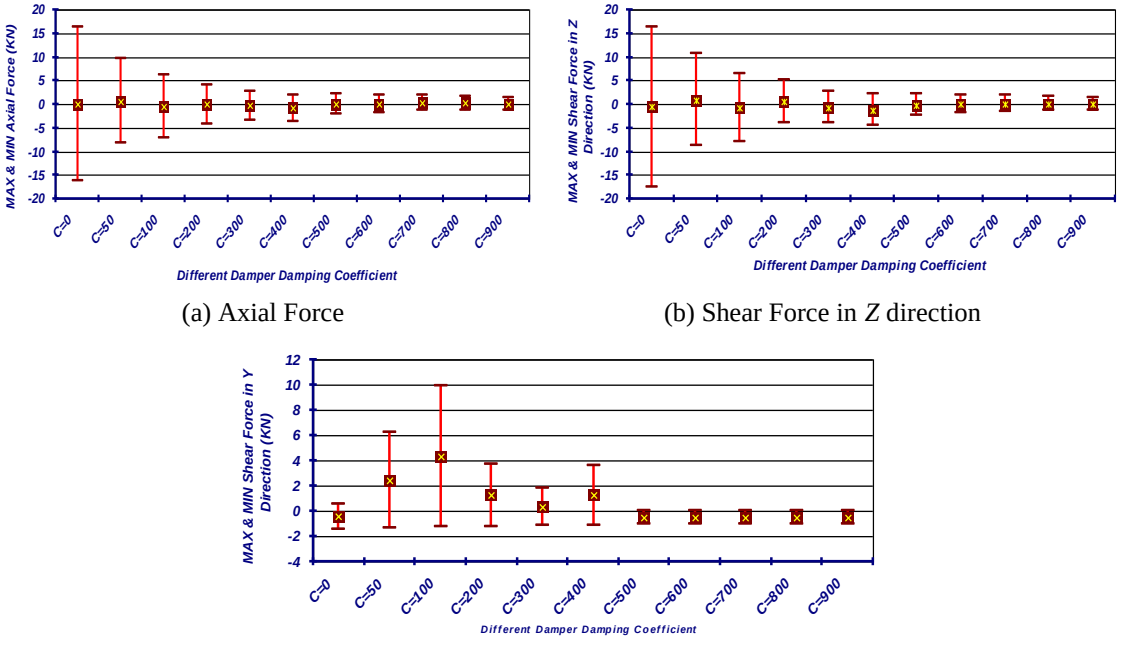

(a) Axial Force

(b) Shear Force in *Z* direction

(c) Shear Force in *Y* direction

Fig. 20 Peak maximum and minimum axial and shear force at structure beams and columns in different damper damping coefficient

supplemental earthquake energy dissipation system is 7.6 kN.mm, increased to 11.8 and 10.8 kN.mm by implementation of VD with *C*=50 and 100 kN.sec/m, respectively. The VD with 200 to 900 kN.sec/m coefficient resulted in the range for peak moment in direction Z decreasing; this amount is minimized to 1.8 when *C*=900 kN.sec/m. This indicates a 76 percent reduction in moment in direction *Z*.

The range for peak moment variations around the *Y* direction is plotted in Fig. 21(c) for various damping coefficients. The peak moment for the structure lacking a damper device is 0.95 kN.mm. By increasing the damping coefficient, the peak moment force around *Y* direction falls to 0.17 (kN.mm) for the case with a damping coefficient *C*=900 N.sec/mm, which is equal to an 82 percent reduction.

Fig. 22 shows the time history displacement of the top node in all directions during earthquake excitation for the case where the damping coefficient equals 900 N.sec/mm. The efficiency of the VD in reducing structural movement during earthquake load is obvious. The peak displacement amplitude along direction *X*, shown in Fig. 22(a), in a structure without a damper device is 29.5 mm, while utilizing a VD reduces that to 2.66 mm - a 91 percent reduction. A similar reduction also occurs for movement of the top node in direction *Z*, as shown in Fig. 22(b). Implementation of a VD system attenuates the structure's oscillation in direction Z. The peak amplitude at the top node in direction *Z* is reduced from 34.1 mm to 2.7 mm, a 92 percent reduction. The vertical displacement of the node is plotted in Fig. 22(c). The vertical movement peak amplitude diminished for damping of around 50 to 400 kN.sec/m, but it decreased again from 2.01 mm to 1.01 mm (a 50 percent reduction with *C*=50 kN.sec/mm).

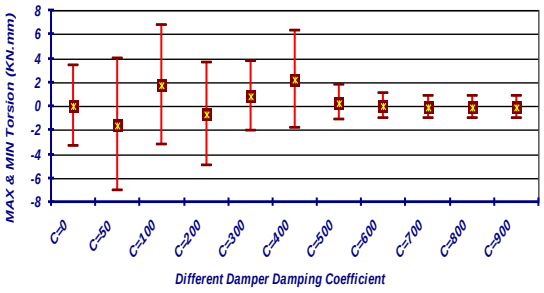

(a) Torsion

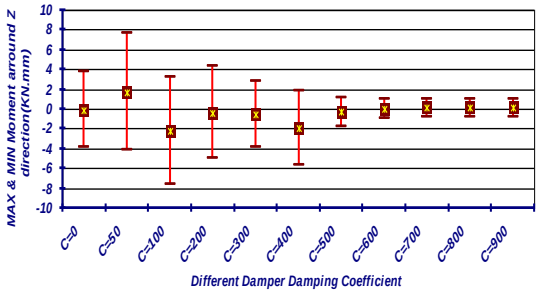

(b) Moment around *Z* direction

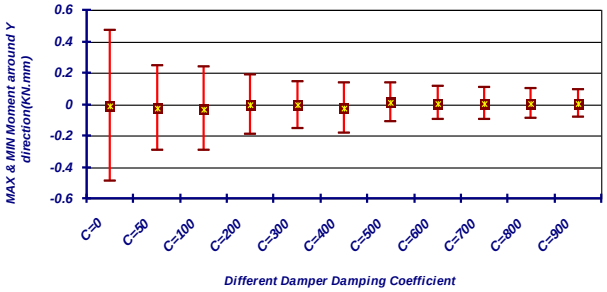

(c) Moment around *Y* direction

Fig. 21 Peak maximum and minimum torsion and moment at structure beams and columns for different damper damping coefficient

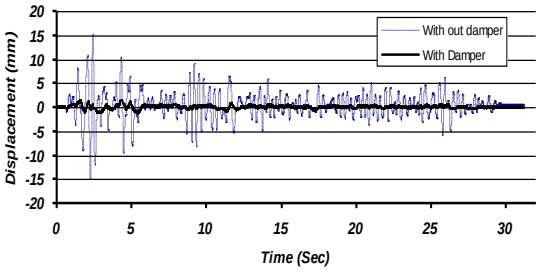

(a) Horizontal displacement in *X* direction

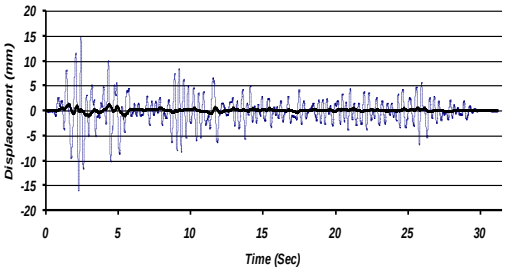

(b) Horizontal displacement in *Z* direction

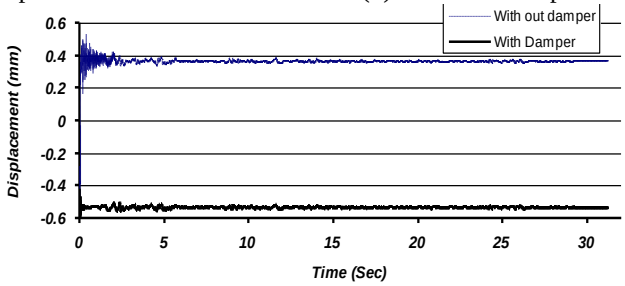

(c) Vertical displacement in *Y* direction

Fig. 22 Time history displacement of structure top node with 900 kN.sec/m damper damping coefficient

Eventually, the seismic response of the structure in terms of the formation of plastic hinges and nodal displacements can be summarized; the average reduction percentage is shown in Table 2 for

different VD damping coefficients. The table indicates that implementing a VD with C=900 kN.sec/m damping coefficient reduces the seismic response of the three-story RC structure, overall, by 91 percent. Therefore, this case can be considered as an optimal damper design for this structure. Results associated with direction Y (vertical) are not presented, due to the small alteration of the displacements compared to the case where no VD device is used.

In general, increase of the damping coefficient associated with damper device led to degradation of plastic hinge occurrence and displacement of the frame in two horizontal direction of X and Z and a continuous declining pattern was observed against the rise of damping coefficient. Comparison of variation percentage of plastic hinge formation showed that reduction of section plastic hinge had greater intensity at lower damping coefficient up to C=400 kN.sec/m with 79 percent reduction while for larger magnitudes of damping coefficient it continued with marginal difference of 6 percent when the damping coefficient reached its peak. Similar trend was found for total plastic hinges formed during the nonlinear dynamic analysis, but with some level of fluctuation for the lower damping coefficients. The declining trend of total plastic hinges got less steep when the damping coefficient grew larger than 500 kN.sec/m after which, only maximum difference of 4 percent was achieved with the maximum damping coefficient.

Reduction of peak maximum displacements along X and Z directions also exhibited a relatively sharp trend for the lower damping coefficients up to 400 kN.sec/m, compared with which, the largest damping coefficient led to only 3.5 and 4.6 percent reduction, respectively. The pattern for peak minimum displacements along X and Z directions happened to have an identical trend compared to that of peak maximum displacement. The peak minimum displacement in X and Z directions associated with C=500 kN.sec/m caused 86 and 87 percent of reduction respectively, compared to that of the frame without damper, while the frame with maximum damping coefficient experienced only 7 percent further reduction of displacement compared with that of

Table 2 Results of structure analysis in various damper damping coefficient

Item	Damper damping coefficient (C) kN.sec/m																				
	0	50	%	100	%	200	%	300	%	400	%	500	%	600	%	700	%	800	%	900	%
Section plastic hinge No	86	45	-48	39	-55	28	-67	18	-79	18	-79	16	-81	16	-81	15	-83	14	-84	14	-84
Total plastic hinge No	384	202	-47	290	-24	144	-63	69	-82	77	-80	36	-91	33	-91	21	-95	20	-95	21	-95
Peak Maximum displ. in X direction (mm)	16.1	9.66	-40	6.07	-62	4.05	-75	2.61	-84	1.96	-88	2.05	-87	1.83	-89	1.74	-89	1.60	-90	1.40	-91
Peak Minimum displ. in X direction (mm)	-16.1	-8.38	-48	-7.09	-56	-4.14	-74	-3.38	-79	-3.76	-77	-2.25	-86	-1.77	-89	-1.45	-91	-1.31	-92	-1.26	-92
Peak Maximum displ. in Z direction (mm)	16.3	10.6	-35	6.33	-61	5.06	-69	2.68	-84	2.15	-87	2.07	-87	1.85	-89	1.77	-89	1.61	-90	1.42	-91
Peak Minimum displ. in Z direction (mm)	-17.7	-8.80	-50	-8.05	-55	-3.98	-78	-4.01	-77	-4.66	-74	-2.34	-87	-1.87	-89	-1.51	-91	-1.36	-92	-1.28	-93
Average percentage			-45		-52		-71		-81		-81		-87		-88		-90		-90		-91

C=500 kN.sec/m.

Comparison between the averages showed that although the frame with *C*=300 and 400 kN.sec/m provided similar trends of seismic response, however, the damper with *C*=500 kN.sec/m led to better performance associated with 6 percent average larger reduction of seismic behavior. Nevertheless, the results showed that the behavior of frame can be even more improved with larger damping forces correspond to *C*=900 kN.sec/m.

10. Conclusions

The developed model for VDs, the associated finite element algorithm, and the program code were applied to a 3D RC frame structure to demonstrate the performance of the proposed system. Comparing the seismic responses of the system without an energy dissipation device to the structure equipped with the proposed VD elements showed that the incorporation of these damper devices efficiently modified the structural response when subjected to earthquakes forces.

The results reveal that VDs can reasonably influence the structural displacement and the formation of plastic hinges in a structure's sections. By evaluating the effects of damper parameters on the seismic response of structures, an optimum design for an earthquake energy dissipation system can be proposed. The criterion of being optimum and reasonable design in this study were considered as reduction of structural member forces and story displacements regardless of economical or other practical stand points of view such as fabrication of damper device with 900 kN.sec/m damping coefficient. Appropriate damper properties for the desired design of the structure can be selected based on the needed structural performance as well as the probable maximum effect of the damper device on reducing seismic load. Therefore, based on the obtained results, the following conclusions are achieved:

• Implementation of a damper device effectively reduces the linear response or displacement of a structure during earthquake excitation.

• Nonlinear responses of a structure as to plastic hinges formation and structure movements are reduced by the use of dampers.

• Increasing the damper damping coefficient enhances earthquake energy dissipation, reducing subsequent damage to the building.

• Using VDs on two sides of a building affects all associated responses of a space frame structure (two horizontal and one vertical) under multidirectional earthquake excitation.

• The optimum design of damper parameters is possible by evaluating how the damper damping coefficient affects the structure's response, and VDs with the desired damper properties can be manufactured accordingly.

Acknowledgments

This work received financial support from the Ministry of Higher Education of Malaysia under FRGS Research Projects No. 5524254 and No. 5524256 and was further supported by the University Putra Malaysia under Putra grant No. 9415100. These supports are gratefully acknowledged.

References

Akhaveissy, A.H. and Desai, C.S. (2012), "Application of the DSC model for nonlinear analysis of reinforced concrete frames", *Finite Elem. Anal. Des.*, **50**, 98-107.

Athanassiadou, C. (2008), "Seismic performance of R/C plane frames irregular in elevation", *Eng. Struct.*, **30**(5), 1250-1261.

Birely, A.C., Lowes, L.N. and Lehman, D.E. (2012), "A model for the practical nonlinear analysis of reinforced-concrete frames including joint flexibility", *Eng. Struct.*, **34**, 455-465.

Buyukozturk, O. and Connor, J.J. (1978), "Nonlinear dynamic response of reinforced concrete under impulsive loading: Research status and needs", *Nucl. Eng. Des.*, **50**(1), 83-92.

Chandler, A. and Mendis, P. (2000), "Performance of reinforced concrete frames using force and displacement based seismic assessment methods", *Eng. Struct.*, **22**(4), 352-363.

Cruz, M.F. and López, O.A. (2004), "Design of reinforced concrete frames with damage control", *Eng. Struct.*, **26**(14), 2037-2045.

Constantinou, M. and Symans, M. (1993), "Experimental study of seismic response of buildings with supplemental fluid dampers", *Struct. Des. Tall Build.*, **2**(2), 93-132.

de Lautour, O.R. and Omenzetter, P. (2009), "Prediction of seismic-induced structural damage using artificial neural networks", *Eng. Struct.*, **31**(2), 600-606.

Dong, P., Moss, P.J. and Carr, A.J. (2003), "Seismic structural damage assessment of reinforced concrete ductile framed structures", *Pacific Conference on Earthquake Engineering*.

Erduran, E. (2008), "Assessment of current nonlinear static procedures on the estimation of torsional effects in low-rise frame buildings", *Eng. Struct.*, **30**(9), 2548-2558.

Eurocode 8 (1998), *Design of structures for earthquake resistance*, Part **1**, 1998-1991.

Faisal, A., Majid, T.A. and Hatzigeorgiou, G.D. (2013), "Investigation of story ductility demands of inelastic concrete frames subjected to repeated earthquakes", *Soil Dyn. Earthq. Eng.*, **44**, 42-53.

Faleiro, J., Oller, S. and Barbat, A. (2008), "Plastic-damage seismic model for reinforced concrete frames", *Comput. Struct.*, **86**(7), 581-597.

Ganjavi, B. and Hao, H. (2012), "A parametric study on the evaluation of ductility demand distribution in multi-degree-of-freedom systems considering soil-structure interaction effects", *Eng. Struct.*, **43**, 88-104.

Godínez-Domínguez, E.A. and Tena-Colunga, A. (2010), "Nonlinear behavior of code-designed reinforced concrete concentric braced frames under lateral loading", *Eng. Struct.*, **32**(4), 944-963.

Grassl, P. and Jirásek, M. (2006), "Damage-plastic model for concrete failure", *Int. J. Solid. Struct.*, **43**(22), 7166-7196.

Habibi, A. and Izadpanah, M. (2012), "New method for the design of reinforced concrete moment resisting frames with damage control", *Scientia Iranica*, **19**(2), 234-241.

Habibi, A. and Moharrami, H. (2010), "Nonlinear sensitivity analysis of reinforced concrete frames", *Finite Elem. Anal. Des.*, **46**(7), 571-584.

Hakim, S.J.S. and Razak, H.A. (2013), "Adaptive Neuro Fuzzy Inference System (ANFIS) and Artificial Neural Networks (ANNs) for structural damage identification", *Struct. Eng. Mech.*, **45**(6), 779-802.

Hakim, S.J.S. and Razak, H.A. (2014), "Frequency response function-based structural damage identification using artificial neural networks-a review", *Res. J. Appl. Sci., Eng. Technol.*, **7**(9), 1750-1764.

Hatzigeorgiou, G.D. and Liolios, A.A. (2010), "Nonlinear behaviour of RC frames under repeated strong ground motions", *Soil Dyn. Earthq. Eng.*, **30**(10), 1010-1025.

Hejazi, F., Kojouri, S.J., Noorzaei, J., Jaafar, M., Thanoon, W. and Abdullah, A. (2011), "Inelastic seismic response of RC building with control system", *Key Eng. Mater.*, **462**, 241-246.

Hejazi, F., Noorzaei, J., Jaafar, M. and Abdullah, A.A. (2009), "Earthquake analysis of reinforce concrete framed structures with added viscous dampers", *Int. J. Appl. Sci., Eng. Technol.*, **5**(4), 205-210.

Hejazi, F., Zabihi, A. and Jaafar, M. (2014), "Development of elasto-plastic viscous damper finite element model for reinforced concrete frames", *Soil Dyn. Earthq. Eng.*, **65**, 284-293.

Hueste, M.B.D. and Bai, J.W. (2007), "Seismic retrofit of a reinforced concrete flat-slab structure: Part I-

seismic performance evaluation", *Eng. Struct.*, **29**(6), 1165-1177.
Hwang, J.S. (2002), "Seismic design of structures with viscous dampers", *Int. Train. Progr. Seism. Des. Build. Struct.*
Inel, M. and Ozmen, H.B. (2006), "Effects of plastic hinge properties in nonlinear analysis of reinforced concrete buildings", *Eng. Struct.*, **28**(11), 1494-1502.
Jiang, H., Chen, L. and Chen, Q. (2011), "Seismic damage assessment and performance levels of reinforced concrete members", *Procedia Eng.*, **14**, 939-945.
Karayannis, C.G., Favvata, M.J. and Kakaletsis, D. (2011), "Seismic behaviour of infilled and pilotis RC frame structures with beam-column joint degradation effect", *Eng. Struct.*, **33**(10), 2821-2831.
Krätzig, W.B. and Pölling, R. (2004), "An elasto-plastic damage model for reinforced concrete with minimum number of material parameters", *Comput. Struct.*, **82**(15), 1201-1215.
Lagaros, N.D. and Papadrakakis, M. (2012), "Neural network based prediction schemes of the non-linear seismic response of 3D buildings", *Adv. Eng. Soft.*, **44**(1), 92-115.
Lee, H.S. and Woo, S.W. (2002), "Seismic performance of a 3-story RC frame in a low-seismicity region", *Eng. Struct.*, **24**(6), 719-734.
Lee, J.Y., Kim, J.Y. and Oh, G.J. (2009), "Strength deterioration of reinforced concrete beam-column joints subjected to cyclic loading", *Eng. Struct.*, **31**(9), 2070-2085.
Lee, J.Y. and Watanabe, F. (2003), "Predicting the longitudinal axial strain in the plastic hinge regions of reinforced concrete beams subjected to reversed cyclic loading", *Eng. Struct.*, **25**(7), 927-939.
Légeron, F., Paultre, P. and Mazars, J. (2005), "Damage mechanics modeling of nonlinear seismic behavior of concrete structures", *J. Struct. Eng.*, **131**(6), 946-955.
Lu, Y. and Wei, J. (2008), "Damage-based inelastic response spectra for seismic design incorporating performance considerations", *Soil Dyn. Earthq. Eng.*, **28**(7), 536-549.
Maheri, M.R. and Ghaffarzadeh, H. (2008), "Connection overstrength in steel-braced RC frames", *Eng. Struct.*, **30**(7), 1938-1948.
Makris, N., Dargush, G. and Constantinou, M. (1993), "Dynamic analysis of generalized viscoelastic fluids", *J. Eng. Mech.*, **119**(8), 1663-1679.
Marante, M. and Flórez-López, J. (2002), "Model of damage for RC elements subjected to biaxial bending", *Eng. Struct.*, **24**(9), 1141-1152.
Massumi, A. and Absalan, M. (2013), "Interaction between bracing system and moment resisting frame in braced RC frames", *Archiv. Civ. Mech. Eng.*, **13**(2), 260-268.
Mata, P., Oller, S. and Barbat, A. (2008), "Dynamic analysis of beam structures considering geometric and constitutive nonlinearity", *Comput. Meth. Appl. Mech. Eng.*, **197**(6), 857-878.
Mehanny, S. and El Howary, H. (2010), "Assessment of RC moment frame buildings in moderate seismic zones: Evaluation of Egyptian seismic code implications and system configuration effects", *Eng. Struct.*, **32**(8), 2394-2406.
Mohr, S., Bairán, J.M. and Marí, A.R. (2010), "A frame element model for the analysis of reinforced concrete structures under shear and bending", *Eng. Struct.*, **32**(12), 3936-3954.
Montuori, R., Nastri, E. and Piluso, V. (2013), "Theory of plastic mechanism control for the seismic design of braced frames equipped with friction dampers", *Mech. Res. Commun.*
Nakhaei, M. and Ali Ghannad, M. (2008), "The effect of soil-structure interaction on damage index of buildings", *Eng. Struct.*, **30**(6), 1491-1499.
NARCBEEEDS (2012), *Program Code for Nonlinear Analysis of Reinforced Concrete Buildings Equipped with Earthquake Energy Dissipation System*, Copyright by University Putra, Malaysia.
Newmark, N.M. (1959), "A method of computation for structural dynamics", *Proc.*, ASCE, **85**(3), 67-94.
Oviedo, A., J.A., Midorikawa, M. and Asari, T. (2010), "Earthquake response of ten-story story-drift-controlled reinforced concrete frames with hysteretic dampers", *Eng. Struct.*, **32**(6), 1735-1746.
Özel, A.E. and Güneyisi, E.M. (2011), "Effects of eccentric steel bracing systems on seismic fragility curves of mid-rise R/C buildings: A case study", *Struct. Saf.*, **33**(1), 82-95.
Park, Y.J. and Ang, A.H.S. (1985), "Mechanistic seismic damage model for reinforced concrete", *J. Struct. Eng.*, **111**(4), 722-739.

Rajeev, P. and Tesfamariam, S. (2012), "Seismic fragilities of non-ductile reinforced concrete frames with consideration of soil structure interaction", *Soil Dyn. Earthq. Eng.*, **40**, 78-86.
Sadjadi, R., Kianoush, M. and Talebi, S. (2007), "Seismic performance of reinforced concrete moment resisting frames", *Eng. Struct.*, **29**(9), 2365-2380.
Sahoo, D.R. and Rai, D.C. (2013), "Design and evaluation of seismic strengthening techniques for reinforced concrete frames with soft ground story", *Eng. Struct.*, **56**, 1933-1944.
Santoro, M.G. and Kunnath, S.K. (2013), "Damage-based RC beam element for nonlinear structural analysis", *Eng. Struct.*, **49**, 733-742.
Schnobrich, W. (1977), "Behavior of reinforced concrete structures predicted by the finite element method", *Comput. Struct.*, **7**(3), 365-376.
Schultz, A.E. (1990), "Experiments on seismic performance of RC frames with hinging columns", *J. Struct. Eng.*, **116**(1), 125-145.
Shinozuka, M., Wen, Y.K. and Casciati, F. (1990), "Seismic damage and damage-control design for RC frames", *J. Intel. Mater. Syst. Struct.*, **1**(4), 476-495.
Soong, T.T. and Costantinou, M.C. (1994), *Passive and active structural vibration control in civil engineering*, Springer-Verlag New York, USA.
Tabatabaiefar, H.R. and Massumi, A. (2010), "A simplified method to determine seismic responses of reinforced concrete moment resisting building frames under influence of soil–structure interaction", *Soil Dyn. Earthq. Eng.*, **30**(11), 1259-1267.
Tena-Colunga, A., Correa-Arizmendi, H., Luna-Arroyo, J.L. and Gatica-Avilés, G. (2008), "Seismic behavior of code-designed medium rise special moment-resisting frame RC buildings in soft soils of Mexico City", *Eng. Struct.*, **30**(12), 3681-3707.
Thanoon, W. (1993), "Inelastic dynamic analysis of concrete frames under non-nuclear blast loading", Ph.D. Dissertation, University of Roorkee, India.
Thanoon, W.A., Paul, D., Jaafar, M.S. and Trikha, D. (2004), "Influence of torsion on the inelastic response of three-dimensional rc frames", *Finite Elem. Anal. Des.*, **40**(5), 611-628.
Wilkinson, S. and Hiley, R. (2006), "A non-linear response history model for the seismic analysis of high-rise framed buildings", *Comput. Struct.*, **84**(5), 318-329.
Xue, Q., Wu, C.W., Chen, C.C. and Chen, K.C. (2008), "The draft code for performance-based seismic design of buildings in Taiwan", *Eng. Struct.*, **30**(6), 1535-1547.
Youssef, M., Ghaffarzadeh, H. and Nehdi, M. (2007), "Seismic performance of RC frames with concentric internal steel bracing", *Eng. Struct.*, **29**(7), 1561-1568.
Zhang, J., Zhang, Z. and Chen, C. (2010), "Yield criterion in plastic-damage models for concrete", *Acta Mechanica Solida Sinica*, **23**(3), 220-230.
Zonta, D., Elgamal, A., Fraser, M. and Nigel Priestley, M. (2008), "Analysis of change in dynamic properties of a frame-resistant test building", *Eng. Struct.*, **30**(1), 183-196.